Depression of an infinite liquid surface by an incompressible gas jet

By W. E. OLMSTEAD AND S. RAYNOR

Department of Mechanical Engineering and Astronautical Sciences, Northwestern University, Evanston, Illinois

(Received 18 October 1963)

The problem of small angle depressions in a liquid surface due to an impinging two-dimensional potential jet is considered. Using conformal mapping methods and finite Hilbert transforms, the problem is formulated as a non-linear singular integral equation. The integral equation is approximated by a set of non-linear algebraic equations which are solved numerically by a method of repeated linear corrections. In addition, an asymptotic solution (for low jet velocity) is derived.

From the numerical solutions of the integral equation, the liquid-surface profiles and the free streamlines of the jet are calculated for four cases. These results verify the appearance of lips on the liquid surface which have been observed experimentally by others.

1. Introduction

Recently, an extensive experimental study of a gas jet impinging on a liquid surface has been carried out by Banks & Chandrasekhara (1963). For the case of low jet velocity, their results show a clearly defined cavity in the liquid which has its maximum depression at the centreline; moving away from the centreline the liquid rises to form a lip and then finally returns to the original level. An inquiry was made whether a simple physical model which assumes potential flow of a two-dimensional gas jet impinging symmetrically on an infinite liquid surface could adequately describe this phenomenon.

Anticipating the use of conformal mapping techniques, some complex variables will be introduced. The Z-plane, or physical plane, is shown in figure 1 and defined by

$$Z = X + iY = \pi(x + iy)/b, \tag{1}$$

where b is the width of the jet at $Y = \infty$. The W-plane, or potential plane, is shown in figure 2(a). Let

$$W = \Phi + i\Psi = \frac{\pi}{V_J b}(\phi + i\psi), \tag{2}$$

where V_J is the jet velocity at $Y = \infty$, and also due to continuity the velocity at $X = \pm\infty$. Noting that the volume flow per unit length of the jet is $V_J b$, it follows that the jet boundaries (free streamlines) may be labelled $\Psi = 0, \pi$. Due to

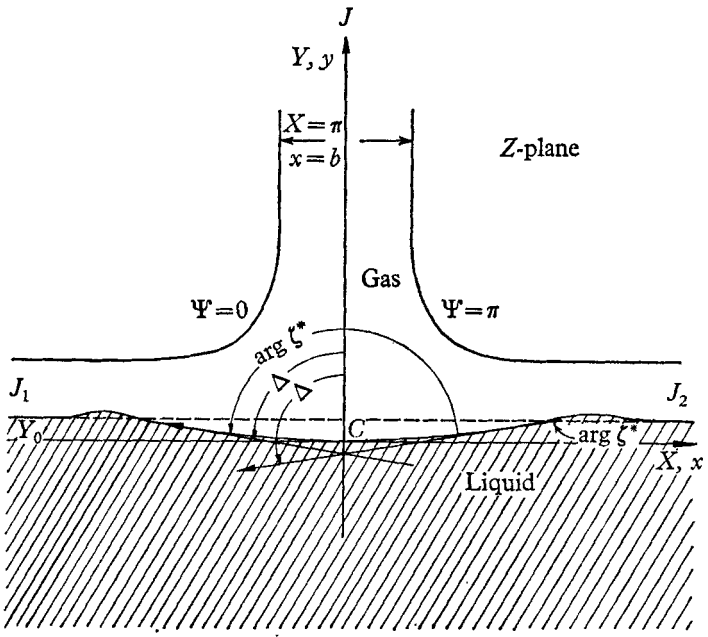

FIGURE 1. The physical plane.

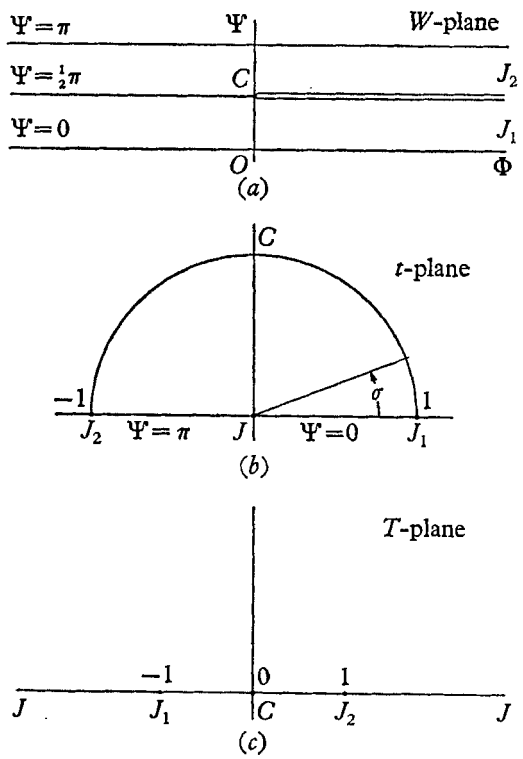

FIGURE 2. Auxiliary planes.

symmetry, the liquid surface may be labelled $\Psi = \frac{1}{2}\pi$, $\Phi \geqslant 0$. Finally, the complex velocity, in non-dimensional form, is defined as

$$\zeta = \frac{1}{V_J}\left(\frac{\partial \phi}{\partial x} + i\frac{\partial \psi}{\partial x}\right). \tag{3}$$

Bernoulli's equation for the gas and the liquid may be expressed as

$$\tfrac{1}{2}\rho_G V_J^2 |\zeta|^2 + P_G = \tfrac{1}{2}\rho_G V_J^2 + P_{\text{atm.}}, \tag{4}$$

$$P_L + \frac{\rho_L g b}{\pi} Y = P_{\text{atm.}} + \frac{\rho_L g b}{\pi} Y_0, \tag{5}$$

where P_G is the local gas pressure, $P_{\text{atm.}}$ is the pressure outside of the jet, P_L is the local liquid pressure, Y_0 is the depression at the centreline, and g is the gravitational constant. Velocity head in the liquid is neglected as compared with gravity head.

2. Formulation in complex variables

The complex potential and complex velocity are related by

$$\zeta = \frac{dW}{dZ}. \tag{6}$$

The boundary condition along the free streamlines is $P_G = P_{\text{atm.}}$. Hence it follows from equation (4) that the boundary condition for ζ along the free streamlines is

$$|\zeta|^2 = 1 \quad \text{on} \quad \Psi = 0, \pi. \tag{7}$$

Along the liquid surface, the requirement is made that $P_G = P_L$ (i.e. surface tension is neglected). From equations (4) and (5) follows

$$|\zeta|^2 = 1 - \frac{4}{\pi\lambda}(Y_0 - Y) \quad \text{on} \quad \Psi = \tfrac{1}{2}\pi, \quad \Phi \geqslant 0, \tag{8}$$

where

$$\lambda = 2\rho_G V_J^2 / \rho_L g b. \tag{9}$$

At the stagnation point, $\zeta = 0$ and $Y = 0$, hence

$$Y_0 = \tfrac{1}{4}\pi\lambda, \tag{10}$$

which determines the centreline depression. The boundary condition (8) along the gas-liquid interface then becomes

$$|\zeta|^2 = \frac{4}{\pi\lambda} Y \quad \text{on} \quad \Psi = \tfrac{1}{2}\pi, \quad \Phi \geqslant 0. \tag{11}$$

The differential equation (6) with boundary conditions (7) and (11) defines the problem. In order to reduce this problem to an integral equation, a method described by Birkhoff & Zarantonello (1957) for jet flow around curved obstacles will be applied. Using this method, the liquid surface will be treated as an obstacle of unknown shape along which boundary condition (11) must hold.

It is convenient to introduce two additional complex planes. In figure 2(*b*) is shown the t-plane in which the flow domain is mapped on to the interior of the semicircle specified by $|t| = |\xi + i\eta| < 1, \quad (\eta > 0).$

The points J_1, J_2, C of the physical plane are mapped on to $1, -1, i$, respectively. Hence the free streamlines are mapped on to the real diameter and the liquid surface on to the curve

$$t = e^{i\sigma} \quad (0 \leqslant \sigma \leqslant \pi).$$

The T-plane, in which the potential plane $W$is mapped on to the upper half-plane, is shown in figure 2(*c*). It provides a convenient link between the W-plane and t-plane. Using the conformal transformations

$$W = -\tfrac{1}{2}\log(T^2-1) + i\pi, \quad T = -\tfrac{1}{2}(t+t^{-1}),$$

equation (6) may be expressed as

$$\frac{dZ}{dt} = \zeta^{-1}(t)\frac{dW}{dt}\frac{dT}{dt} = \frac{1}{t}\left(\frac{1+t^2}{1-t^2}\right)\zeta^{-1}(t).$$

In integral form,

$$Z(t) = \int_i^t \frac{1}{t_1}\left(\frac{1+t_1^2}{1-t_1^2}\right)\zeta^{-1}(t_1)\,dt_1. \tag{12}$$

The complex velocity $\zeta(t)$ is expressed more conveniently as

$$\zeta(t) = i\left(\frac{1+it}{1-it}\right)e^{-i\Omega(t)}. \tag{13}$$

On the liquid surface ($t = e^{i\sigma}$, $0 \leqslant \sigma \leqslant \pi$), the function $(1+it)/(1-it)$ has a jump of π in its argument at $\sigma = \frac{1}{2}\pi$, which accounts for the change in the direction of velocity across the stagnation point C. Furthermore, on the real diameter ($t = \xi$, $-1 \leqslant \xi \leqslant 1$), it follows that $|(1+i\xi)/(1-i\xi)| = 1$. Then expressing the Levi-Civita function Ω as

$$\Omega = \theta + i\tau, \tag{14}$$

it follows from equation (13) that

$$|\zeta(\xi)|^2 = e^{2\tau}.$$

Hence the boundary condition (7) will be satisfied automatically if τ vanishes on the real diameter. As a consequence of this and some additional arguments based on the continuity of the boundary $\widehat{J_1 C J_2}$, Birkhoff & Zarantonello showed that $\Omega(t)$ is continuous in the unit circle $|t| < 1$ and can be expanded in a Taylor series

$$\Omega(t) = \sum_{m=0}^{\infty} a_m t^m, \tag{15}$$

where all a_m are real.

On the liquid surface ($t = e^{i\sigma}$, $0 \leqslant \sigma \leqslant \pi$), equation (15) becomes

$$\Omega(e^{i\sigma}) = \sum_{m=0}^{\infty} a_m(\cos m\sigma + i\sin m\sigma). \tag{16}$$

Comparing equations (14) and (16) gives

$$\theta(\sigma) = \sum_{m=0}^{\infty} a_m \cos m\sigma, \quad \tau(\sigma) = \sum_{m=1}^{\infty} a_m \sin m\sigma. \tag{17), (18}$$

In a manner analogous to that of Birkhoff & Zarantonello, it can be shown that

$$\theta(\sigma) = \Delta - \tfrac{1}{2}\pi,$$

where Δ is defined as the angle between the positive Y-axis and the tangent to the liquid surface directed so as to have the gas on the right. With this physical interpretation of $\theta(\sigma)$ it follows for reasons of symmetry that

$$\Omega(t) = \sum_{m=1}^{\infty} a_{2m-1} t^{2m-1}, \tag{19}$$

and on $t = e^{i\sigma}$,

$$\theta(\sigma) = \sum_{m=1}^{\infty} a_{2m-1} \cos(2m-1)\sigma, \quad \tau(\sigma) = \sum_{m=1}^{\infty} a_{2m-1} \sin(2m-1)\sigma. \tag{20), (21}$$

Since the boundary condition along the free streamlines has been satisfied, and the formal expansion of Ω for the symmetrical case has been found, it remains only to satisfy the boundary condition (11) along the liquid surface. Using equations (12) and (13) in boundary condition (11) yields

$$\left(\frac{\cos\sigma}{1+\sin\sigma}\right)^2 e^{2\tau(\sigma)} = \frac{4}{\pi\lambda} \operatorname{Im} \int_{\frac{1}{2}\pi}^{\sigma} \left(\frac{1+e^{i2\omega}}{1-e^{i2\omega}}\right) \left(\frac{1-ie^{i\omega}}{1+ie^{i\omega}}\right) e^{i\theta(\omega)+\tau(\omega)} d\omega. \tag{22}$$

After obtaining the imaginary part of the integrand in equation (22) and then differentiating both sides of the equation, the following form is obtained:

$$\frac{d}{d\sigma}\left[\left(\frac{\cos\sigma}{1+\sin\sigma}\right)^3 e^{3\tau(\sigma)}\right] = \frac{6}{\pi\lambda} \cot\sigma \sin\theta(\sigma). \tag{23}$$

In the next section, a mathematical relation between $\tau(\sigma)$ and $\theta(\sigma)$ will be introduced to supplement equation (23) which was derived from the physical model.

3. Additional formulation through finite Hilbert transforms

The following formula is well known in the applications of integral equations, see Tricomi (1957).

$$*\int_0^{\pi} \frac{\cos k\sigma'}{\cos\sigma' - \cos\sigma} d\sigma' = \pi \frac{\sin k\sigma}{\sin\sigma} \quad (k = 0, 1, 2, \ldots), \tag{24}$$

where the asterisk denotes the Cauchy principal integral.

Considering equation (24) for only odd values of k, it follows that

$$*\int_{\frac{1}{2}\pi}^{\pi} \frac{\cos\sigma' \cos(2m-1)\sigma'}{\cos 2\sigma' - \cos 2\sigma} d\sigma' = \frac{\pi}{4} \frac{\sin(2m-1)\sigma}{\sin\sigma} \quad (m = 1, 2, 3, \ldots). \tag{25}$$

In view of the expansions (20) and (21), it follows from equation (25) that

$$\tau(\sigma) = \frac{4\sin\sigma}{\pi} *\int_{\frac{1}{2}\pi}^{\pi} \frac{\cos\sigma'\theta(\sigma')}{\cos 2\sigma' - \cos 2\sigma} d\sigma' \quad \text{on} \quad \widehat{CJ}_2. \tag{26}$$

Thus it is seen that $\tau(\sigma)$ is an integral transform of $\theta(\sigma)$. In particular it is a finite Hilbert transform where the more familiar notation is accomplished by the substitutions

$$r = \cos 2\sigma, \quad s = \cos 2\sigma', \quad \bar{\tau}(r) = \tau(\sigma), \quad \bar{\theta}(s) = \theta(\sigma'). \tag{27}$$

Equation (26) becomes

$$(1-r)^{-\frac{1}{2}}\bar{\tau}(r) = -\frac{1}{\pi}\,{}^{*}\!\int_{-1}^{1} \frac{(1-s)^{-\frac{1}{2}}\bar{\theta}(s)}{s-r}\,ds \quad \text{on} \quad \widehat{CJ}_2. \tag{28}$$

In terms of the change of variables (27), equation (23) becomes

$$\sin\bar{\theta}(r) = \frac{\pi\lambda}{3}(1-r)\frac{d}{dr}\left\{\left[\frac{2^{\frac{1}{2}}-(1-r)^{\frac{1}{2}}}{2^{\frac{1}{2}}+(1-r)^{\frac{1}{2}}}\right]^{\frac{3}{2}} e^{3\bar{\tau}(r)}\right\} \quad \text{on} \quad \widehat{CJ}_2. \tag{29}$$

Before proceeding, the following approximation is made

$$\sin\bar{\theta}(r) \approx \bar{\theta}(r). \tag{30}$$

Physically, this approximation implies that only cases of small cavity tangent angles may be considered. The approximation is made in order to achieve a more desirable form for numerical analysis.

Combining equations (28) and (29) to eliminate $\bar{\theta}(r)$ while utilizing the approximation (30) yields the following integral equation,

$$(1-r)^{-\frac{1}{2}}\bar{\tau}(r) = -\tfrac{1}{3}\lambda\,{}^{*}\!\int_{-1}^{1} \frac{(1-s)^{\frac{1}{2}}\dfrac{d}{ds}\left\{\left[\dfrac{2^{\frac{1}{2}}-(1-s)^{\frac{1}{2}}}{2^{\frac{1}{2}}+(1-s)^{\frac{1}{2}}}\right]^{\frac{3}{2}} e^{3\bar{\tau}(s)}\right\}}{s-r}\,ds. \tag{31}$$

Using the definitions

$$R(r) = -\frac{3\bar{\tau}(r)}{\lambda(1-r)^{\frac{1}{2}}}, \quad S(s) = \left[\frac{2^{\frac{1}{2}}-(1-s)^{\frac{1}{2}}}{2^{\frac{1}{2}}+(1-s)^{\frac{1}{2}}}\right]^{\frac{3}{2}} e^{3\bar{\tau}(s)}, \tag{32}$$

equation (31) may be expressed as

$$R(r) = {}^{*}\!\int_{-1}^{1} \frac{\dfrac{d}{ds}[(1-s)^{\frac{1}{2}}S(s)]}{s-r}\,ds + \frac{1}{2}\,{}^{*}\!\int_{-1}^{1} \frac{(1-s)^{-\frac{1}{2}}S(s)}{s-r}\,ds. \tag{33}$$

Muskhelishvilli (1953) provides the following identity

$${}^{*}\!\int_{-1}^{1} \frac{\Gamma'(s)}{s-r}\,ds = \frac{d}{dr}\,{}^{*}\!\int_{-1}^{1} \frac{\Gamma(s)}{s-r}\,ds, \quad \Gamma(1) = \Gamma(-1) = 0. \tag{34}$$

By noting that $[(1-s)^{\frac{1}{2}}S(s)]_{s=\pm 1} = 0$, equation (33) becomes

$$R(r) = \frac{d}{dr}\,{}^{*}\!\int_{-1}^{1} \frac{(1-s)^{\frac{1}{2}}S(s)}{s-r}\,ds + \frac{1}{2}\int_{-1}^{1} \frac{(1-s)^{-\frac{1}{2}}S(s)}{s-r}\,ds. \tag{35}$$

Consider now another identity

$$\frac{d}{dr}\,{}^{*}\!\int_{-1}^{1} \frac{(1-s)^{\frac{1}{2}}G(s)}{s-r}\,ds = \frac{d}{dr}\left[(1-r)\,{}^{*}\!\int_{-1}^{1} \frac{(1-s)^{-\frac{1}{2}}G(s)}{s-r}\,ds\right],$$

which can be easily verified by inserting the definition of the principal integral and carrying out the differentiation. Using this identity and multiplying equation (35) by $(1-r)^{-\frac{1}{2}}$ yields the form

$$(1-r)^{-\frac{1}{2}}R(r) = \frac{d}{dr}\left[(1-r)^{\frac{1}{2}}\,{}^{*}\!\int_{-1}^{1} \frac{(1-s)^{-\frac{1}{2}}S(s)}{s-r}\,ds\right]. \tag{36}$$

Substituting the definitions (32) for R and S, equation (36) becomes

$$\bar{\tau}(r) = -\tfrac{1}{3}\lambda(1-r)\frac{d}{dr}\,{}^{*}\!\int_{-1}^{1}\left(\frac{1-r}{1-s}\right)^{\frac{1}{2}}\frac{\left[\dfrac{2^{\frac{1}{2}}-(1-s)^{\frac{1}{2}}}{2^{\frac{1}{2}}+(1-s)^{\frac{1}{2}}}\right]^{\frac{3}{2}}e^{3\bar{\tau}(s)}}{s-r}\,ds. \tag{37}$$

Ultimately, equation (37) will be solved numerically for $\bar{\tau}(r)$. Formally, once $\bar{\tau}$ has been found then $\bar{\theta}$ can be obtained from equation (29). An alternate expression for $\bar{\theta}$ comes from inverting the finite Hilbert transform of equation (28). Using one of the inversion formulae (see Tricomi) it follows from equation (28) that

$$\bar{\theta}(r) = \frac{1}{\pi}\,{}^{*}\!\int_{-1}^{1}\left(\frac{1-r}{1-s}\right)^{\frac{1}{2}}\left(\frac{1-r^2}{1-s^2}\right)^{\frac{1}{2}}\frac{\bar{\tau}(s)}{s-r}\,ds \quad \text{on} \quad \widehat{CJ}_2. \tag{38}$$

4. Equations for the physical variables

In order to determine the liquid surface profiles, the following change of variables will provide a more convenient scale for the numerical analysis:

$$\nu^4 = \tfrac{1}{2}(1-r), \quad \mu^4 = \tfrac{1}{2}(1-s), \quad f(\nu) = -3\bar{\tau}(r), \quad \tilde{\theta}(\nu) = \bar{\theta}(r). \tag{39}$$

Under this change of variables, the singular integral equation (37) for $\bar{\tau}$ becomes

$$f(\nu) = \lambda\nu\frac{d}{d\nu}\,{}^{*}\!\int_{0}^{1}\frac{\nu^2\mu\left(\dfrac{1-\mu^2}{1+\mu^2}\right)^{\frac{3}{2}}e^{-f(\mu)}}{\mu^4-\nu^4}\,d\mu \quad (0 \leqslant \nu \leqslant 1). \tag{40}$$

Equations (29) and (38) for $\bar{\theta}$ become

$$\tilde{\theta}(\nu) = \frac{4}{3\pi}\,{}^{*}\!\int_{0}^{1}\frac{\nu^4}{\mu}\left(\frac{1-\nu^4}{1-\mu^4}\right)^{\frac{1}{2}}\frac{f(\mu)}{\mu^4-\nu^4}\,d\mu \quad \text{on} \quad \widehat{CJ}_2. \tag{41}$$

$$\tilde{\theta}(\nu) = -\frac{\pi\lambda}{12}\nu\frac{d}{d\nu}\left[\left(\frac{1-\nu^2}{1+\nu^2}\right)^{\frac{3}{2}}e^{-f(\nu)}\right] \quad \text{on} \quad \widehat{CJ}_2. \tag{42}$$

The set of parametric equations for the liquid surface profiles follows from equations (11), (12) and (13) with changes of variables given by (27) and (39),

$$\frac{\bar{y}(\nu)}{b} = \frac{\lambda}{4}\left(\frac{1-\nu^2}{1+\nu^2}\right)e^{-\frac{3}{2}f(\nu)}, \tag{43}$$

$$\frac{\bar{x}(\nu)}{b} = \frac{2}{\pi}\int_{\nu}^{1}\left(\frac{1+\mu^2}{1-\mu^2}\right)^{\frac{1}{2}}\frac{e^{\frac{1}{2}f(\mu)}\cos\tilde{\theta}(\mu)}{\mu}\,d\mu \quad \text{on} \quad \widehat{CJ}_2. \tag{44}$$

Once $f(\nu)$ and $\tilde{\theta}(\mu)$ are known, then equations (43) and (44) yield the liquid surface profile.

The pressure distribution along the liquid surface follows from Bernoulli's equation (5) as

$$\frac{P_L - P_{\text{atm.}}}{\rho_L g b} = \frac{\lambda}{4}\left[1-\left(\frac{1-\nu^2}{1+\nu^2}\right)e^{-\frac{3}{2}f(\nu)}\right]. \tag{45}$$

The net vertical force F_v exerted on the liquid surface by the impinging jet can be found by integrating the pressure distribution,

$$F_v = 2\int_0^{\infty}(P_L - P_{\text{atm.}})\,d\bar{x}.$$

Utilizing equations (44) and (45) the expression for F_v becomes

$$\frac{F_v}{\rho_L g b^2} = \frac{\lambda}{2}\int_0^1 \frac{2}{\pi}\cos\tilde{\theta}(\mu)\,\frac{(1+\mu^2)\,e^{\frac{1}{2}f(\mu)} - (1-\mu^2)\,e^{-\frac{1}{2}f(\mu)}}{\mu(1-\mu^4)^{\frac{1}{2}}}\,d\mu. \tag{46}$$

The force on the surface may also be obtained by elementary momentum considerations as

$$F_v = \rho_G b V_J^2.$$

Then from the definition of λ follows

$$\frac{F_v}{\rho_L g b^2} = \frac{\lambda}{2}. \tag{47}$$

Comparison of equations (46) and (47) shows that the integral in equation (46) must be equal to unity. This condition will be used later as an estimate of the error in the numerical analysis.

The free streamlines ($\Psi = 0, \pi$) have been mapped on to the real diameter of the semicircle: $t = \xi$, $-1 \leqslant \xi \leqslant 1$. Designating $(\hat{x}, \hat{y})$ as the co-ordinates of a point on a free streamline, it follows from equations (6) and (13) that

$$\frac{\pi}{b}(d\hat{x} + i\,d\hat{y}) = -\frac{i}{\xi}\left(\frac{1-i\xi}{1+i\xi}\right)\left(\frac{1+\xi^2}{1-\xi^2}\right)e^{i\Omega(\xi)}\,d\xi. \tag{48}$$

After separating equation (48) into real and imaginary parts, a change of variables $\alpha = -\xi$ is made, and then integrating the differential expressions using the reference values $x = \frac{1}{2}b$ at $\xi = 0$ and $y = \frac{1}{2}(1+\frac{1}{2}\lambda)\,b$ at $\xi = -1$, it follows that

$$\frac{\hat{x}(a)}{b} = \frac{1}{2} + \frac{1}{\pi}\int_0^\alpha \left(\frac{2\cos\Omega(\omega)}{1-\omega^2} - \frac{\sin\Omega(\omega)}{\omega}\right)d\omega \quad (0 \leqslant \alpha \leqslant 1), \tag{49}$$

$$\frac{\hat{y}(\alpha)}{b} = \frac{1}{2}\left(1+\frac{\lambda}{2}\right) + \frac{1}{\pi}\int_\alpha^1 \left(\frac{2\sin\Omega(\omega)}{1-\omega^2} - \frac{\cos\Omega(\omega)}{\omega}\right)d\omega \quad (0 \leqslant \alpha \leqslant 1). \tag{50}$$

Once $\Omega(\omega)$ is known these equations constitute a set of parametric equations for the free streamline $\Psi = \pi$. To compute the free streamlines, the coefficients a_{2m-1}, from which follows Ω, must be known. These coefficients follow directly from the expansions (21) and (22) as

$$a_{2m-1} = \frac{4}{\pi}\int_0^{\frac{1}{2}\pi} \theta(\sigma)\cos(2m-1)\,\sigma\,d\sigma = \frac{4}{\pi}\int_0^{\frac{1}{2}\pi} \tau(\sigma)\sin(2m-1)\,\sigma\,d\sigma, \tag{51}$$

5. A limiting case and checks on the numerical solution

A limiting case of the problem considered is that of a two-dimensional jet impinging symmetrically on a flat plate; see, for example, Milne-Thomson (1960). Infinite liquid density ($\lambda = 0$) corresponds to this case since the liquid surface profile degenerates into a straight line, i.e. $\theta(\sigma) \equiv 0$. Hence from equation (51) follows

$$\lim_{\lambda \to 0} a_{2m-1} = 0 \quad (m = 1, 2, 3, \ldots). \tag{52}$$

Applying condition (52) to the free streamline equations (49) and (50) gives

$$\lim_{\lambda\to 0}\left[\frac{\hat{x}(\alpha)}{b}\right] = \frac{1}{2}+\frac{1}{\pi}\log\left(\frac{1+\alpha}{1-\alpha}\right), \tag{53}$$

$$\lim_{\lambda\to 0}\left[\frac{\hat{y}(\alpha)}{b}\right] = \frac{1}{2}-\frac{1}{\pi}\log\alpha. \tag{54}$$

This parametric representation is equivalent to the form given by Milne-Thomson for jet impingement on a flat plate.

For very small values of λ (and hence very slight depressions) an asymptotic solution for $f(\nu)$ will be derived in §7. This asymptotic solution will be compared with the numerical results of §8 as a check. Another check on the numerical work was mentioned in §4, namely that the integral in equation (46) should be equal to unity. Still another possible check comes from the condition of zero slope for the liquid profile at $X = \pm\infty$, i.e. $\theta(0) = \theta(\pi) = 0$. In view of expansion (20) this leads to the following criterion for the Fourier coefficients,

$$\sum_{m=1}^{\infty} a_{2m-1} = 0. \tag{55}$$

6. End-point evaluations

Some useful information about the behaviour of $f(\nu)$ at the end-points $\nu = 0, 1$ can be obtained. From physical arguments, $\bar{y}(0)/b = \frac{1}{4}\lambda$. Hence from equation (43) follows

$$f(0) = 0. \tag{56}$$

In order to determine $f'(0)$, equation (43) was evaluated at $\nu = 0$ utilizing the property (56). This gives

$$f'(0) = \frac{12}{\pi\lambda}\lim_{\nu\to 0}\frac{\tilde{\theta}(\nu)}{\nu}.$$

Then using the integral expression (41) for $\tilde{\theta}(\nu)$ it follows that

$$f'(0) = 0. \tag{57}$$

In the singular integral equation (40) for $f(\nu)$, the differentiation generally cannot be performed under the integral sign because the integrand is not continuous. However, at $\nu = 1$ the integrand is continuous, and therefore carrying out the differentiation and evaluating equation (40) yields

$$f(1) = 2\lambda\int_0^1 \frac{\mu(1+\mu^4)\,e^{-f(\mu)}}{(1+\mu^2)^3\,(1-\mu^4)^{\frac{1}{2}}}\,d\mu. \tag{58}$$

Equation (58) does not give $f(1)$ explicitly, but this form will prove to be useful in the numerical analysis.

7. Asymptotic solution for $f(\nu)$

As $\rho_L \to \infty$, or equivalently $\lambda \to 0$, the liquid surface profile approaches a straight line. Under this condition the limit for $f(\nu)$ follows directly from condition (52) and expansion (21) as

$$\lim_{\lambda\to 0} f(\nu) = 0.$$

Consequently, equation (40) suggests the asymptotic form

$$f(\nu) \sim \lambda\nu \frac{d}{d\nu} {}^{*}\int_0^1 \frac{\nu^2\mu\left(\frac{1-\mu^2}{1+\mu^2}\right)^{\frac{3}{2}}}{\mu^4-\nu^4}\,d\mu \quad \text{for} \quad \lambda \ll 1. \tag{59}$$

Utilizing the indefinite integral

$$\int \frac{\nu^2\mu\left(\frac{1-\mu^2}{1+\mu^2}\right)^{\frac{3}{2}}}{\mu^4-\nu^4}\,d\mu = \frac{1-p^4(\nu)}{2p^2(\nu)}\left\{q(\mu) - \frac{1}{2p(\nu)\,[1-p^4(\nu)]} \times \left[\log\left|\frac{1+p(\nu)\,q(\mu)}{1-p(\nu)\,q(\mu)}\right| - p^6(\nu)\log\left|\frac{p(\nu)+q(\mu)}{p(\nu)-q(\mu)}\right|\right]\right\},$$

where $$p(\nu) = \left(\frac{1-\nu^2}{1+\nu^2}\right)^{\frac{1}{2}}, \quad q(\mu) = \left(\frac{1-\mu^2}{1+\mu^2}\right)^{\frac{1}{2}},$$

the asymptotic solution for $f(\nu)$ follows from (59) as

$$f(\nu) \sim \frac{\lambda}{8}\frac{[1-p^4(\nu)]}{p^4(\nu)}\left\{2[3+p^2(\nu)+3p^4(\nu)] - \frac{3[1+p^6(\nu)]}{p(\nu)}\log\left[\frac{1+p(\nu)}{1-p(\nu)}\right]\right\} \quad \text{for} \quad \lambda \ll 1. \tag{60}$$

For the asymptotic solution it can be shown that $f(0) = f'(0) = 0$, which agrees with the general results found in § 6; and $f(1) = 3\lambda/5$. This solution is particularly useful for low jet velocity.

8. Numerical analysis

The central problem of the numerical analysis is the determination of $f(\nu)$ from the integral equation (40). Once $f(\nu)$ is known the remaining quantities of physical interest follow directly.

To approximate the Cauchy principal integral in this equation, first separate the integral into the two parts, then specify ϵ to be small and disregard the limit notation, i.e.

$${}^{*}\int_0^1 K(\nu,\mu)\,e^{-f(\mu)}\,d\mu \approx \left(\int_0^{\nu-\epsilon} + \int_{\nu+\epsilon}^1\right) K(\nu,\mu)\,e^{-f(\mu)}\,d\mu, \tag{61}$$

where $$K(\nu,\mu) = \frac{\nu^2\mu\left(\frac{1-\mu^2}{1+\mu^2}\right)^{\frac{3}{2}}}{\mu^4-\nu^4}.$$

Proceeding further with the approximation, the two integrals will be approximated by trapezoidal rule with the interval of integration being specified as ϵ; hence for N equal intervals $\epsilon = 1/N$. Then equation (61) becomes

$${}^{*}\int_0^1 K(\nu,\mu)\,e^{-f(\mu)}\,d\mu \approx \frac{1}{N}\sum_{k=1}^{N} \gamma_{j,k} K_{j,k} e^{-f_k} \quad (j = 1, 2, \ldots N), \tag{62}$$

where $$\gamma_{j,k} = \begin{cases} 0, & k = j, \\ 1/2, & k = j \pm 1 \quad (j \neq N), \\ 1, & \text{otherwise}, \end{cases} \tag{63}$$

and where $K_{j,k} = K(j/N, k/N)$ and $f_k = f(k/N)$. This type of approximtion has been used previously by Birkhoff (1956). Using this approximation and also employing finite differences yields the following set of non-linear algebraic equations for f_j,

$$f_j = \lambda \sum_{k=1}^{N} K^*_{j,k} e^{-f_k} \quad (j = 1, 2, \ldots, N), \tag{64}$$

where

$$K^*_{j,k} = \begin{cases} 0, & k = N, \quad j \neq N, \\ L_k, & j = N, \\ \dfrac{j}{N}(\gamma_{j+1,k} K_{j+1,k} - \gamma_{j,k} K_{j,k}), & \text{otherwise}, \end{cases} \tag{65}$$

and

$$L_k = \begin{cases} \frac{1}{2} N^{-\frac{1}{2}}, & k = N, \\ \dfrac{N^2(N-1)\,[N^4 + (N-1)^4]}{[N^2 + (N-1)^2]^3\,[N^4 - (N-1)^4]^{\frac{1}{2}}}, & k = N-1, \\ \dfrac{2N^2 k (N^4 + k^4)}{(N^2 + k^2)^3\,(N^4 - k^4)^{\frac{1}{2}}}, & \text{otherwise}. \end{cases}$$

In (65) the special evalution of $K^*_{j,k}$ for $j = N$ arises from the approximation of equation (58) for f_N. It should be pointed out here that, without the approximation $\sin\theta \approx \theta$, the resulting numerical form equivalent to equation (64) would have contained differences in the exponentials of the unknown functions f_k, which is a much less desirable form.

In order to compute f_j, a method of direct iteration was tried first; however, this method yielded very slow convergence or no convergence at all for $\lambda > 0{\cdot}3$. Consequently, the following method of repeated linear corrections was adopted. Let f^0_j be an approximate solution of equation (64). Then define

$$f_j = f^0_j + f'_j, \tag{66}$$

where f'_j is a set of corrections to the approximate solution. For $|f'_j| \ll 1$, the following approximation is suggested:

$$e^{-f_k} \approx e^{-f^0_k}(1 - f'_k). \tag{67}$$

Substituting equations (66) and (67) in equation (64) yields the following set of linear equations for the corrections f'_j:

$$f'_j + \lambda \sum_{k=1}^{N} K^*_{j,k} e^{-f^0_k} f'_k = \lambda \sum_{k=1}^{N} K^*_{j,k} e^{-f^0_k} - f^0_j. \tag{68}$$

A solution of the equation (68) can generally be found since λ is a specified physical parameter and in general the determinant of $\delta_{j,k} + \lambda K^*_{j,k} e^{-f^0_k}$ will not vanish.

Once the set of corrections f'_j is found and added to f^0_j, a new approximation of f_j is obtained. This procedure can be repeated until the corrections are sufficiently small.

Using this method, values of f_j were calculated for the cases of $\lambda = 0{\cdot}10$, $0{\cdot}30$, $0{\cdot}50$, $0{\cdot}80$ and $1{\cdot}00$. In each case, the initial choice of an approximate

solution was $f_j^0 = 0$. The number of integration intervals was $N = 20$ (i.e. $\epsilon = 0{\cdot}05$) and the criterion for stopping the correction procedure was $\max|f_j'| < 0{\cdot}0001$. (It is noteworthy that no more than five repetitions were required for the cases considered.) The numerical results are represented graphically in figure 3.

The asymptotic solution (60) for $f(\nu)$ was evaluated for $\lambda = 0{\cdot}10$ and is also shown in figure 3. Comparison with the corresponding numerical solution indicates good agreement. The asymptotic solution is slightly above in the range

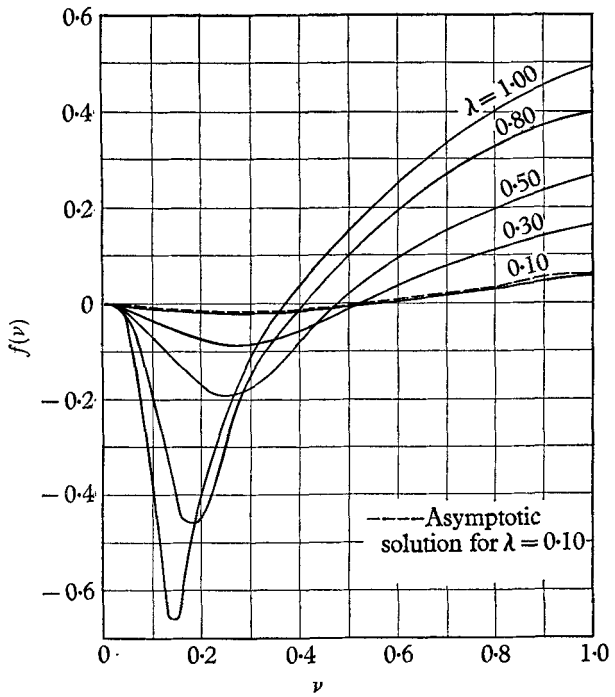

FIGURE 3. Numerical solutions for $f(\nu)$.

$0{\cdot}80 < \nu < 0{\cdot}90$, but at $\nu = 1{\cdot}0$ there is again very close agreement owing to the more accurate approximation at this point.

Using the numerical results for $f(\nu)$, the vertical co-ordinate of the liquid surface profile $\bar{y}(\nu)/b$ follows immediately from equation (43). The horizontal co-ordinate $\bar{x}(\nu)/b$ was found by numerical integration of equation (44) with $\tilde{\theta}(\nu)$ being evaluated by a finite difference approximation of equation (42). The results for the liquid surface profiles are shown in figures 4–7.

As mentioned previously, the integral in the vertical force equation (46) should be unity. This integral can be evaluated from the numerical results for $f(\nu)$. Hence these evaluations provide an estimate of the error in the results for $f(\nu)$. Defining the error as

$$\text{Error} = 1 - (2F_v/\lambda\rho_L g b^2) \text{ calculated},$$

the results are displayed in table 1.

In order to calculate the free streamlines it is necessary to know the coefficients a_{2m-1} so that $\Omega(\alpha)$ may be found from equation (19). From equations (39) and (51) follows

$$a_{2m-1} = -\frac{4}{3\pi}\int_0^{\frac{1}{2}\pi} f[\nu(\sigma)]\sin(2m-1)\,\sigma\,d\sigma, \tag{69}$$

where $$\nu(\sigma) = (\sin\sigma)^{\frac{1}{2}}.$$

Using the results for $f(\nu)$ displayed in figure 3, the first fifteen coefficients were determined by numerical integration of equation (69). These results are some-

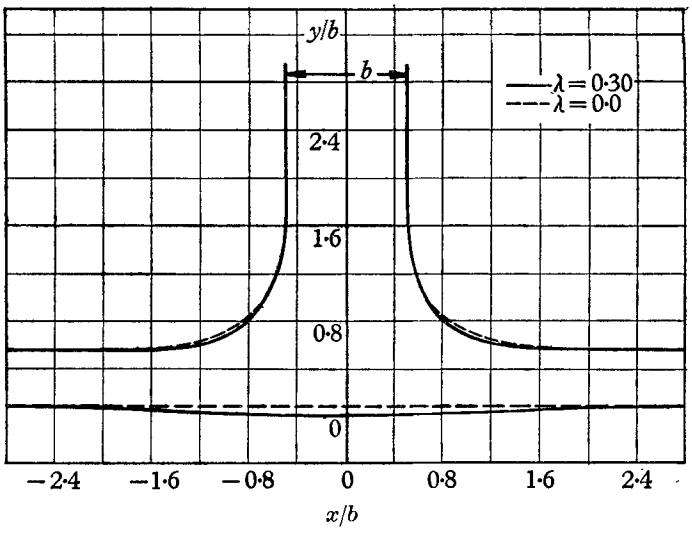

FIGURE 4. Free streamlines and liquid surface profile for $\lambda = 2\rho_G V_J^2/\rho_L g b = 0{\cdot}3$.

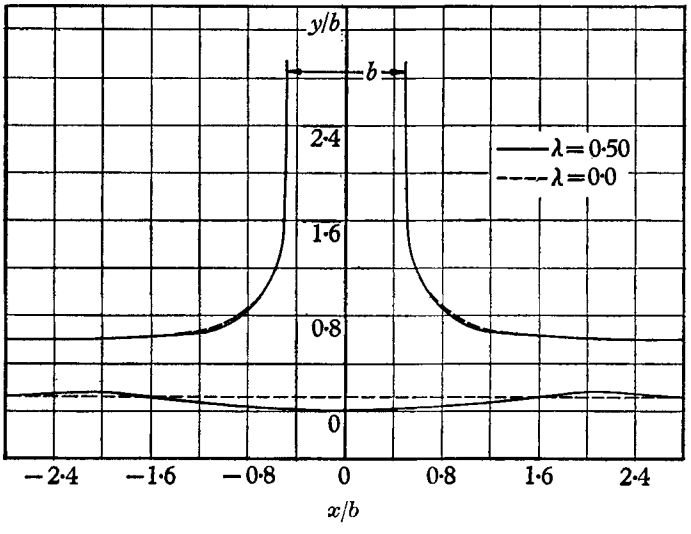

FIGURE 5. Free streamlines and liquid surface profile for $\lambda = 2\rho_G V_J^2/\rho_L g b = 0{\cdot}5$.

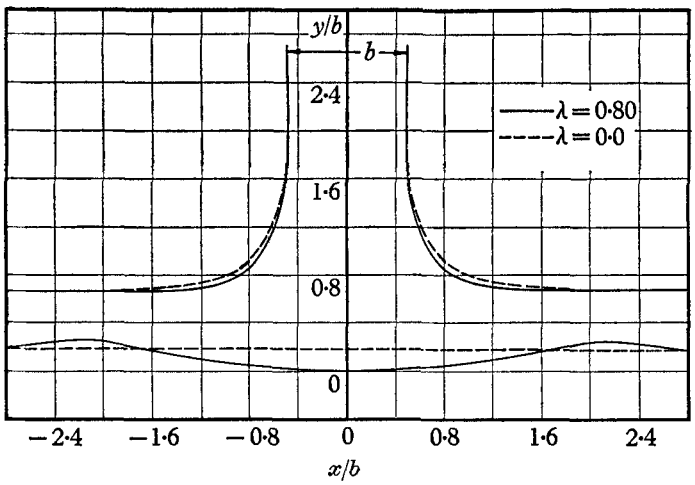

FIGURE 6. Free streamlines and liquid surface profile for $\lambda = 2\rho_G V_J^2/\rho_L g b = 0{\cdot}8$.

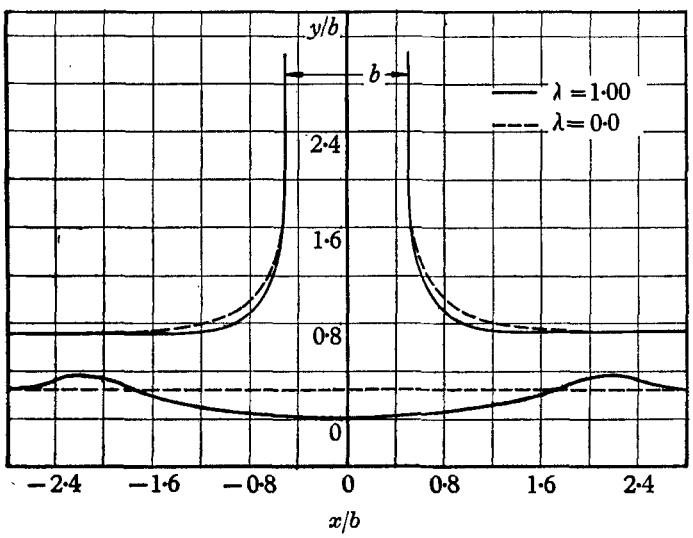

FIGURE 7. Free streamlines and liquid surface profile for $\lambda = 2\rho_G V_J^2/\rho_L g b = 1{\cdot}0$.

λ	Error (%)
0·10	0·0
0·30	1·1
0·50	2·4
0·80	5·1
1·00	7·6

TABLE 1. Estimate of error based on calculation of the vertical force on the liquid.

what lengthy for presentation here; however, it should be mentioned that the results do show consistency with condition (55).

In order to achieve a suitable numerical form of the free-streamline equations (49) and (50), the integrals are first separated as

$$\frac{\hat{x}(\alpha)}{b} = \frac{1}{2} + \frac{1}{\pi}\left\{\int_0^{\alpha} \frac{2\cos\Omega(\omega)}{1-\omega^2}\,d\omega - \int_0^{\delta} \frac{\sin\Omega(\omega)}{\omega}\,d\omega - \int_{\delta}^{\alpha} \frac{\sin\Omega(\omega)}{\omega}\,d\omega\right\}, \tag{70}$$

$$\frac{\hat{y}(\alpha)}{b} = \frac{1}{2}\left(1+\frac{\lambda}{2}\right) + \frac{1}{\pi}\left\{\int_{\alpha}^{1} \frac{\cos\Omega(\omega)}{\omega}\,d\omega + 2\int_{\alpha}^{1-\delta} \frac{\sin\Omega(\omega)}{1-\omega^2}\,d\omega + 2\int_{1-\delta}^{1} \frac{\sin\Omega(\omega)}{1-\omega^2}\,d\omega\right\}, \tag{71}$$

where $0 < \delta \ll 1$. The second integral in equation (70) and the last integral in equation (71) have integrands which take on an indeterminant form at $\omega = 0$ and $\omega = 1$ respectively. To evaluate these indeterminant forms, no method of evaluation may be used which requires differentiation of $\Omega(\omega)$ since there is no assurance that the differentiated series converges. In the first case an approximation can be made as follows:

$$\int_0^{\delta} \frac{\sin\Omega(\omega)}{\omega}\,d\omega \approx \int_0^{\delta} \frac{\Omega(\omega)}{\omega}\,d\omega = \sum_{m=1}^{\infty} \frac{a_{2m-1}}{2m-1}\,\delta^{2m-1}.$$

In equation (71), set $\alpha = 1-\delta$. Since δ is small, $\hat{y}(1-\delta)/b$ corresponds to a very large value of $\hat{x}/b$. It is assumed that $\hat{y}(1-\delta)/b$ is essentially the same as for the flat plate solution. Thus it follows from equations (71) and (54) that

$$2\int_{1-\delta}^{1} \frac{\sin\Omega(\omega)}{1-\omega^2}\,d\omega \frac{1}{2}\int_{1-\delta}^{1} \frac{\Omega^2(\omega)}{\omega}\,d\omega \approx \frac{[\Omega(1-\delta)]^2}{4}.$$

Since $\Omega(1-\delta) \ll 1$, the contribution is negligible. Using these two approximations and numerical integration of the remaining integrals, the free streamlines were calculated. The results are shown in figures 4–7. In these calculations, it was found that consideration of only the first six Fourier coefficients a_{2m-1} was sufficient.

9. Discussion of numerical results

The numerical results of figures 4–7 are given for values of $\lambda = 0{\cdot}30$, $0{\cdot}50$, $0{\cdot}80$ and $1{\cdot}00$ respectively. Also the results for the jet impinging on a plate ($\lambda = 0$) are shown on each figure for comparison. For an air jet impinging on water, the case of $\lambda = 1{\cdot}0$ could, for example, correspond to: $\rho_L/\rho_G = 815$, $b = 0{\cdot}5$ in. and $V_J = 23{\cdot}4$ ft./sec. Lower values of λ may be conveniently thought of as applying to lower values of V_J.

In the results for the surface profiles, it can be seen that as λ increases the centreline depression increases and the lips on the surface become more prominent and more slightly outward. This has been observed experimentally by Banks & Chandrasekhara. Using their definition of cavity width as the distance between the two lip peaks, the ratio of cavity width to cavity depth at the centreline was calculated from figures 5–7. These results are tabulated in table 2. It is difficult to make a comparison with the experimental results of Banks &

Chandrasekhara since their values of cavity width to cavity height are plotted against a parameter equivalent to $\lambda b^2/2H^2$ where H is the jet height above the liquid surface. For the problem considered here, H is infinite. However, the values of table 2 appear to be qualitatively consistent with their data for large values of H, i.e. $H/b \geqslant 10$.

λ	Cavity width/ cavity height
0·5	31·5
0·8	21·0
1·0	17·5

TABLE 2. Ratio of cavity width to cavity height.

The free streamline results of figures 4–7 show the tendency of the jet to extend further without spreading than in the case of the flat plate. This is to be expected since the surface is depressed below the original level.

10. Conclusion

The simple physical model of a potential flow gas jet impinging on a motionless liquid surface has yielded results which agree with the experimental results for cases considered.

The authors would like to thank the Northwestern University Computing Center, whose establishment was made possible by the National Science Foundation, for the use of the IBM 709. In addition, thanks are due to the National Science Foundation and Northwestern University for fellowship support of one of the authors (W. E. O.).

REFERENCES

BANKS, R. B. & CHANDRASEKHARA, D. V. 1963 *J. Fluid Mech.* **10**, 13.

BIRKHOFF, G. 1956 *Los Alamos Sci. Lab. Report* LA-1927.

BIRKHOFF, G. & ZARANTONELLO, E. H. 1957 *Jets, Wakes and Cavities*, p. 130. New York: Academic Press.

MILNE-THOMSON, L. M. 1960 *Theoretical Hydrodynamics*, p. 291. London: Macmillan.

MUSKHELISHVILLI, N. I. 1953 *Singular Integral Equations*, p. 376. Gronigen: P. Noordhoff N.V.

TRICOMI, F. G. 1957 *Integral Equations*, p. 173. New York: Interscience.